CrossMark

VVV CL001: Likely the Most Metal-poor Surviving Globular Cluster in the Inner Galaxy

José G. Fernández-Trincado[1,2,3] , Dante Minniti[4,5] , Stefano O. Souza[6] , Timothy C. Beers[7] , Doug Geisler[8,9,10] ,
Christian Moni Bidin[11], Sandro Villanova[8] , Steven R. Majewski[12] , Beatriz Barbuy[6] , Angeles Pérez-Villegas[13] ,
Lady Henao[8] , María Romero-Colmenares[14] , Alexandre Roman-Lopes[9] , and Richard R. Lane[1]

[1] Instituto de Astronomía y Ciencias Planetarias, Universidad de Atacama, Copayapu 485, Copiapó, Chile; jose.fernandez@uda.cl
[2] Institut Utinam, CNRS UMR 6213, Université Bourgogne-Franche-Comté, OSU THETA Franche-Comté, Observatoire de Besançon, BP 1615, F-25010 Besançon Cedex, France
[3] Centro de Investigación en Astronomía, Universidad Bernardo O Higgins, Avenida Viel 1497, Santiago, Chile
[4] Departamento de Cs. Físicas, Facultad de Ciencias Exactas, Universidad Andrés Bello, Av. Fernández Concha 700, Las Condes, Santiago, Chile
[5] Vatican Observatory, V-00120 Vatican City State, Italy
[6] Universidade de São Paulo, IAG, Rua do Matão 1226, Cidade Universitária, São Paulo 05508-900, Brazil
[7] Department of Physics and JINA Center for the Evolution of the Elements, University of Notre Dame, Notre Dame, IN 46556, USA
[8] Departamento de Astronomía, Casilla 160-C, Universidad de Concepción, Concepción, Chile
[9] Department of Astronomy—Universidad de La Serena—Av. Juan Cisternas, 1200 North, La Serena, Chile
[10] Instituto de Investigación Multidisciplinario en Ciencia y Tecnología, Universidad de La Serena. Benavente 980, La Serena, Chile
[11] Instituto de Astronomía, Universidad Católica del Norte, Av. Angamos 0610, Antofagasta, Chile
[12] Department of Astronomy, University of Virginia, Charlottesville, VA 22904, USA
[13] Instituto de Astronomía, Universidad Nacional Autónoma de México, Apdo. Postal 106, 22800 Ensenada, B.C., México
[14] Centro de Astronomía (CITEVA), Universidad de Antofagasta, Av. Angamos 601, Antofagasta, Chile

Abstract

We present the first high-resolution abundance analysis of the globular cluster VVV CL001, which resides in a region dominated by high interstellar reddening toward the Galactic bulge. Using H-band spectra acquired by the Apache Point Observatory Galactic Evolution Experiment, we identified two potential members of the cluster, and estimated from their Fe I lines that the cluster has an average metallicity of $[\text{Fe/H}] = -2.45$ with an uncertainty due to systematics of 0.24 dex. We find that the light-(N), α-(O, Mg, Si), and Odd-Z (Al) elemental abundances of the stars in VVV CL001 follow the same trend as other Galactic metal-poor globular clusters. This makes VVV CL001 possibly the most metal-poor globular cluster identified so far within the Sun's galactocentric distance and likely one of the most metal-deficient clusters in the Galaxy after ESO280-SC06. Applying statistical isochrone fitting, we derive self-consistent age, distance, and reddening values, yielding an estimated age of $11.9^{+3.12}_{-4.05}$ Gyr at a distance of $8.22^{+1.84}_{-1.93}$ kpc, revealing that VVV CL001 is also an old GC in the inner Galaxy. The Galactic orbit of VVV CL001 indicates that this cluster lies on a halo-like orbit that appears to be highly eccentric. Both chemistry and dynamics support the hypothesis that VVV CL001 could be an ancient fossil relic left behind by a massive merger event during the early evolution of the Galaxy, likely associated with either the Sequoia or the Gaia–Enceladus–Sausage structures.

Unified Astronomy Thesaurus concepts: Globular star clusters (656); Chemical abundances (224); Red giant branch (1368)

1. Introduction

The inner[15] Milky Way (MW) contains a significant population of globular clusters (GCs) with a wide range of metallicities ($-2.37 < [\text{Fe/H}] \lesssim 0$; Harris 1996, 2010 edition), most of which are still poorly explored due to the large foreground extinction and high field-star densities that complicate the analysis, especially at low Galactic latitudes. These limitations have been mitigated with wide field near-infrared imaging such as the Vista Variables in the Via Lactea survey (VVV), and its extension the VVVX survey (Minniti et al. 2010; Smith et al. 2018), which has expanded the family of Galactic GCs to more than 300 candidates by the inclusion

of objects in the inner Galaxy (see e.g., Minniti et al. 2017a, 2017b; Palma et al. 2019; Garro et al. 2020), including those in the bulge (D. Geisler et al. 2021, in preparation).

In this context, the high-resolution ($R > 22,0000$) capabilities of the near-IR multifiber spectrographs of the Apache Point Observatory Galactic Evolution Experiment (APOGEE-2; Majewski et al. 2017) allow measurement of new parameters (radial velocity, metallicity, and detailed chemical abundances for many species) with high precision for a large number of Galactic GCs in a homogeneous way (see, e.g., Mészáros et al. 2015, 2020; Schiavon et al. 2017; Fernández-Trincado et al. 2019d, 2020e; Masseron et al. 2019).

Very metal-poor GCs are preferentially associated with the oldest components of galaxies, and are often used as cosmic clocks to track the enrichment history of their host galaxy (Geisler et al. 1995). Thus, beyond the intrinsic scientific value of identifying such ancient objects, the measurements of their chemical composition can therefore provide insight into the build-up of the chemical elements in the earliest epoch of the Milky Way.

---

[15] Here the term "inner" refers to objects distributed inside the Sun's galactocentric distance.
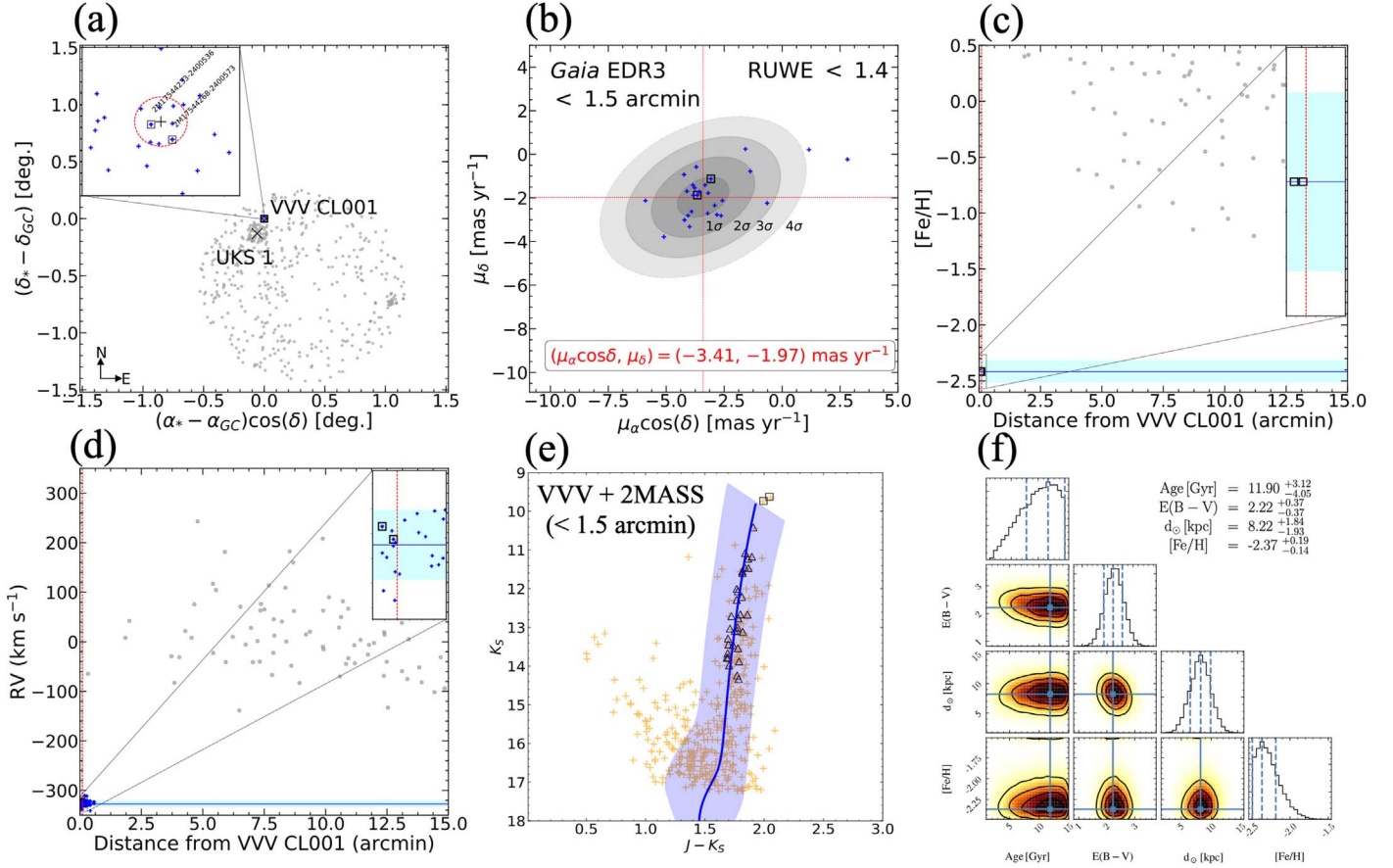
Figure 1. Panel (a): the spatial distribution of APOGEE-2 stars (gray dots) observed toward VVV CL001. The red dashed circle highlights a radius of $0'.1$ centered on VVV CL001 for reference. The black open squares indicate the member candidates in the innermost regions of VVV CL001 from APOGEE-2, while the blue symbols indicate the stars with RV information compiled in Baumgardt & Hilker (2018). The GC UKS 1, with its respective tidal radius, is also overplotted for reference. Panel (b): the Gaia EDR3 proper motion distribution of our sample. The symbols are the same as in panel (a). The concentric ellipses highlight the best-fit distribution after a $3 - \sigma$ clip, with red dotted lines showing the best-fit proper motion of VVV CL001, listed at the bottom of the panel. Panels (c) and (d): metallicities and radial distribution of APOGEE-2 stars (gray dots) and Baumgardt's RV compilation (see Section 4) in the field surrounding VVV CL001. The blue horizontal line and shadowed cyan region indicate the nominal metallicity and RV of VVV CL001 within ± 0.1 dex and ± 6.6 km s^{-1}, respectively. The vertical red dashed lines at $0'.1$ are highlighted for reference. Panel (e): the best isochrone fit in the K_s vs. $(J - K_s)$ CMD using DSED models, where the blue line shows the most probable solution and the blue shadowed region indicates the solutions within $1 - \sigma$. The orange symbols mark the potential candidates from the VVV survey, while the black open squares and triangles refer to stars with RV information from APOGEE-2 and Baumgardt's compilation, respectively. Panel (f): the posterior distributions of the indicated quantities.

To date, the most metal-poor MW GC known is ESO280-SC06 (located ∼15 kpc from the Galactic center), with an estimated metallicity of [Fe/H] = $-2.48^{+0.06}_{-0.11}$ (Simpson 2018), and associated to the Gaia–Enceladus–Sausage (GES; Massari et al. 2019). Here, we report another possible extreme case, VVV CL001, which becomes possibly the most metal-poor GC known inside the Sun's Galactocentric distance, and likely the most metal-poor GC in the Galaxy. It has survived the strong tidal field of the inner MW during its interaction, and its existence implies that GCs below that of the empirical metallicity floor (e.g., Larsen et al. 2020; Wan et al. 2020) have been formed, but only a few exceptional cases have survived during Galactic evolution.

In this Letter, we make use of APOGEE-2 spectra to provide the first spectroscopic study of VVV CL001.

2. Observational Data

We use an interim release data product of the APOGEE-2 survey (Majewski et al. 2017) part of the Sloan Digital Sky Survey IV (SDSS-IV; Blanton et al. 2017) that includes data taken after the release of DR16 (Ahumada et al. 2020), to investigate, for the first time, the chemical composition of VVV CL001.

The (300-fiber) APOGEE instruments are high-resolution ($R \sim 22,500$), near-infrared spectrographs (Wilson et al. 2019) observing all the components of the MW (halo, disk, and bulge/bar) from the Northern Hemisphere on the 2.5 m telescope at Apache Point Observatory (APO, APOGEE-2N; Gunn et al. 2006) and from the Southern Hemisphere on the Irénée du Pont 2.5 m telescope (Bowen & Vaughan 1973) at Las Campanas Observatory (APOGEE-2S). Each instrument records most of the H band (1.51–1.69 μm). See Nidever et al. (2015), García Pérez et al. (2016), and Holtzman et al. (2018) for details regarding the data reduction process and standard stellar parameter estimates. As of 2020 February, the dual APOGEE-2 instruments have observed some ∼600,000 sources across the MW, targeting these stars according to methods described in Zasowski et al. (2013, 2017), with updates to the targeting plan described in R. Beaton et al. (2021, in preparation) and F. Santana et al. (2021, in preparation).

The present study focuses on VVV CL001, a GC discovered by the VVV survey (see, e.g., Minniti et al. 2011). This GC lies in the direction of the Galactic bulge, and is strongly dominated by large foreground extinction, $E(B - V) \gtrsim 2.0$ mag
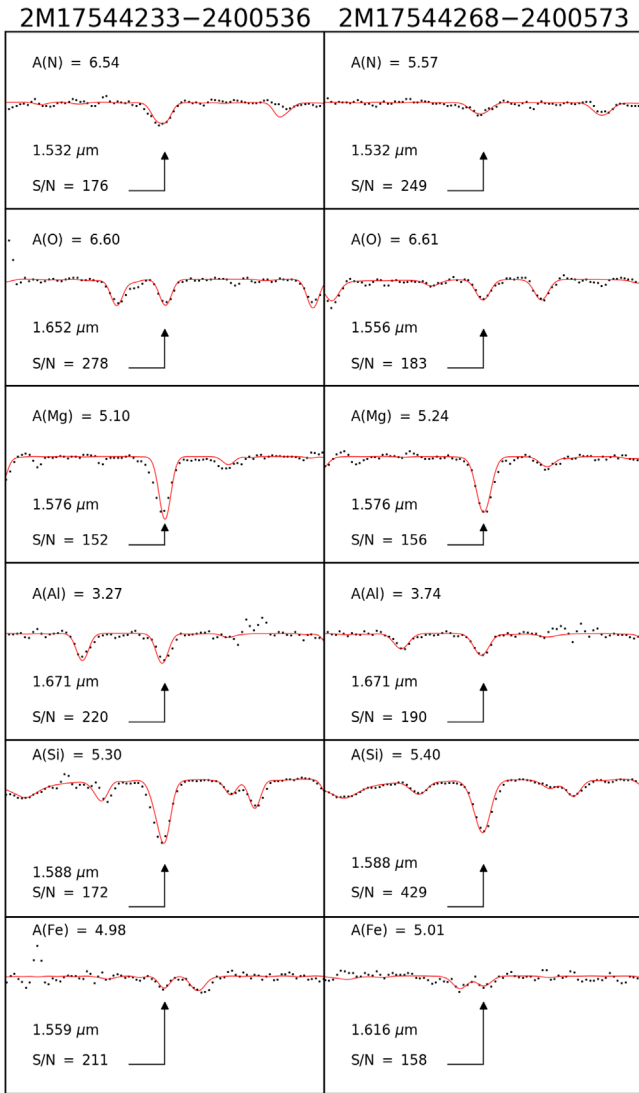
2M17544233−2400536   2M17544268−2400573

Figure 2. Detection of atomic and molecular lines. Spectral synthesis is shown for the determination of the [N/Fe], [O/Fe], [Mg/Fe], [Al/Fe], [Si/Fe], and [Fe/H] abundances for two stars in the innermost regions of VVV CL001. Each panel shows the best-fit syntheses (red line) from BACCHUS compared to the observed spectra (black squares) of selected lines (black arrows).

(Minniti et al. 2011), hampering the observations of this object in the optical bands.

VVV CL001 stars fall on the same APOGEE-2 plug-plates as those associated with the very nearby GC UKS 1, as shown in panel (a) of Figure 1 (see also Fernández-Trincado et al. 2020e, for details regarding to UKS 1); however, the high radial velocities (RVs) of potential VVV CL001 members allow us to cleanly distinguish the UKS 1 sources from VVV CL001 stars. Thus, two high-confidence VVV CL001 members, based on proper motions (see panel (b) of Figure 1) from Gaia Early Data Release 3 (Gaia EDR3: Gaia Collaboration et al. 2020), location in the color–magnitude diagrams (CMDs), and RVs from APOGEE-2 were identified $\lesssim 0\farcm 1$ from the cluster center.

Panels (c) and (d) of Figure 1 show that both our derived [Fe/H] and RV of the VVV CL001 stars are clearly distinct as compared to the foreground and background stars (hereafter, field stars). The [Fe/H] and RVs are at least 1.5 dex and $\sim 150\,\mathrm{km\,s^{-1}}$ offset from the field stars, respectively. Both of these offsets are very large and imply that VVV CL001 is a truly extreme GC. The

Table 1
Atmospheric Parameters and Elemental Abundances of Stars in VVV CL001

APOGEE-ID	2M17544233 −2400536	2M17544268 −2400573
T_{eff} (K)	4100	4200
$\log g$ (cgs)	0.50	0.50
ξ_t (km s^{-1})	1.81	1.69
S/N (pixel^{-1})	229	193
RV (km s^{-1})	−323.57	−326.16
RV-scatter (km s^{-1})	2.55	2.13
[N/Fe]	+1.23 ± 0.31	+0.23 ± 0.40
[O/Fe]	+0.41 ± 0.18	+0.39 ± 0.16
[Mg/Fe]	+0.04 ± 0.02	+0.15 ± 0.09
[Al/Fe]	−0.63 ± 0.11	−0.19 ± 0.09
[Si/Fe]	+0.26 ± 0.14	+0.33 ± 0.10
[Fe/H]	−2.47 ± 0.24	−2.44 ± 0.24

Note. The errors were determined in the same manner as described in Fernández-Trincado et al. (2020a) by varying the atmospheric parameters one at a time by the typical, albeit conservative, values of $\Delta T_{\mathrm{eff}} = \pm 100$ K, $\Delta \log g = \pm 100$ cgs, and $\Delta \xi_t = \pm 0.05$ km s^{-1}. Thus, the reported uncertainties are defined as $\sigma^2_{\mathrm{total}} = \sigma^2_{[\mathrm{X/H}], T_{\mathrm{eff}}} + \sigma^2_{[\mathrm{X/H}], \log g} + \sigma^2_{[\mathrm{X/H}], \xi_t} + \sigma^2_{\mathrm{mean}}$.

two potential cluster members from APOGEE-2 are red giant branch (RGB) stars close to the tip of the giant branch as shown in panel (e) of Figure 1.

In order to have a self-consistent method for age derivation via statistical isochrone fitting, we use the SIRIUS code (Souza et al. 2020), and the most probable cluster members in the VVV catalog located inside $1\farcm 5$ from the cluster center and that have proper motions compatible with that of VVV CL001, as well as those sources with RVs information (see Section 4), which have been marked as open triangle (for Baumgardt's data set) and square (for APOGEE-2 data set) symbols in panel (e) of Figure 1. Due to the quality of our data, we applied some assumptions to obtain an age distribution: a uniform prior in age between 1 and 15 Gyr combined with a slow drop above the age of the universe (13.7 Gyr; Planck Collaboration et al. 2016); the metallicity was varied around the value determined with high-resolution spectroscopy in the present work; the isochrone is limited to $\log g < 4.5$ representing the RGB region. We dereddened and extinction-corrected the VVV+2MASS Ks_s and $J − K_s$ colors with the bulge-specific reddening maps from Gonzalez et al. (2011, 2012) assuming the reddening law of Cardelli et al. (1989). We also noticed that in an $\sim 2' \times 2'$ area the differential reddening across the field does not affect the CMD of VVV CL001, with a negligible variation of 0.03 mag in K_s. Finally, we adopted the Dartmouth Stellar Evolutionary Database (DSED; Dotter et al. 2008) isochrones with $[\alpha/\mathrm{Fe}] = +0.4$ and canonical helium. Panels (e) and (f) of Figure 1 present the best isochrone fits in the K_s versus $(J − K_s)$ CMD. Our fit provides a reasonable solution both in the overplotted isochrone (panel (e)) and the posterior distributions of the corner plot (panel (f)). To represent the distributions, we adopt the median as the most probable value and the uncertainties calculated from the 16th and 84th percentiles. We found an age of $11.9^{+3.12}_{-4.05}$ Gyr and a probable distance of $\sim 8.22^{+1.84}_{-1.93}$ kpc. Also, we want to stress that without the adopted assumptions, the internal error of the age determination could increase and not give a clear age distribution. Consequently, our probable solutions, within $1 − \sigma$, fit well the central part of the CMD, providing confidence that the age estimate is a reasonable determination for VVV CL001.
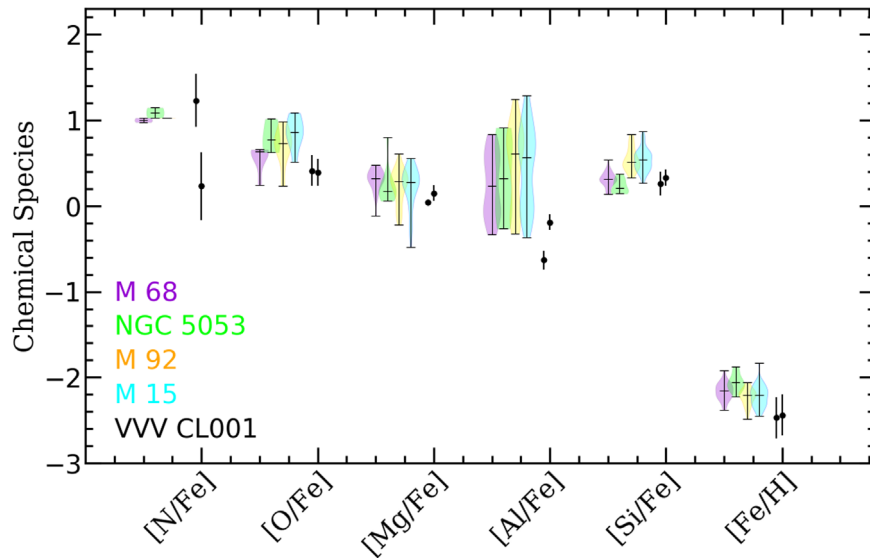
Figure 3. Elemental abundance of stars in VVV CL001 (black symbols) and four comparison metal-poor GCs. Each violin representation show the univariate kernel density estimate of the abundance ratios of each cluster as determined from Mészáros et al. (2020). Each GC has been slightly offset horizontally to distinguish them.

3. Elemental Abundances

As the ASPCAP/APOGEE-2 pipeline (García Pérez et al. 2016) does not provide [Fe/H] and [X/Fe] determinations for VVV CL001 stars, we followed the same technique as described in Fernández-Trincado et al. (2019a, 2019b, 2019c, 2019d, 2020a, 2020b, 2020c, 2020e), and carried out a consistent chemical-abundance analysis for the two VVV CL001 stars with the BACCHUS code (Masseron et al. 2016). The spectra of our sample, in general, have a signal-to-noise ratio (S/N) that is appropriate for elemental-abundance determinations; see Table 1. The atmospheric parameters (T_{eff}, $\log g$, and ξ_t), metallicity ([Fe/H]), and elemental-abundance ratios ([X/Fe]) were derived with the BACCHUS code.

Figure 2 shows the good quality of the APOGEE-2 spectrum compared to the best-fit synthetic spectra for selected atomic and molecule lines of the two stars in VVV CL001, from which the chemical-abundance ratios were determined. For each spectrum we were able to identify reliable lines for six chemical species (N, O, Mg, Al, Si, and Fe). The same figure also reveals the scarcely detectable Fe I lines. The resulting elemental-abundance ratios are listed in Table 1.

The resulting chemical abundances are also displayed in Figure 3, and compared to four GCs at similar metallicity taken from the APOGEE-2 GC sample of Mészáros et al. (2020). We find that the two program stars exhibit an iron abundance ratio of −2.47 to −2.44, suggesting that VVV CL001 has a mean metallicity [Fe/H] = −2.45, with an uncertainty due to systematics of 0.24 dex, which makes this cluster possibly the most metal-poor GC identified so far within the Sun's Galactocentric distance, and with an extreme metallicity close to the apparent "floor" in the empirical metallicity distribution function for GCs in the MW and Local Universe (e.g., Geisler et al. 1995; Simpson 2018; Kruijssen 2019; Larsen et al. 2020; Wan et al. 2020). Note that VVV CL001 has the lowest Fe abundance among this sample, which includes the lowest metallicity GCs observed by APOGEE. With our limited sample, we do not find evidence of an intrinsic Fe-abundance spread.

Regarding the α-elements (O, Mg, and Si), VVV CL001 displays a modest α-element enhancement, a clear signature of the fast enrichment provided by SNe II events, and compatible with other Galactic metal-poor GCs at similar metallicity (see Figure 3). Furthermore, no Mg–Al anticorrelation is evident in our small sample; the two VVV CL001 stars exhibit an aluminum deficit, which places them within the definition of first-generation stars according to the criteria developed by Mészáros et al. (2020). However, one star in our sample displays a very high enrichment in nitrogen, and is considered to likely belong to some of the families of second-generation[16] stars with low-aluminum enrichment (see, e.g., Mészáros et al. 2020), indicating the possible evidence for multiple stellar populations (MPs) in VVV CL001. However, we caution the reader that the error bars in either N or Al abundance (or both) are not properly understood or inconclusive; therefore, more cluster members need to be followed-up of in order to confirm or discard the existence of MPs in this VVV CL001.

4. Dynamical Properties

We made use of the state-of-the-art MW model—Grav-Pot16 to predict the orbital path of VVV CL001 in a steady-state gravitational Galactic model that includes a "boxy/peanut" bar structure.

For the orbit computations, we adopt the same Galactic model configuration, solar position, and velocity vector as described in Fernández-Trincado et al. (2020d), except for the angular velocity of the bar, for which we employed the recommended value of 41 km s^{-1} kpc^{-1} (Sanders et al. 2019).

The most likely orbital parameters and their uncertainties are estimated using a simple Monte Carlo approach. An ensemble of 10,000 orbits were calculated under variations of the observational parameters according to their estimated errors (assumed as $1 - \sigma$ variation), where the errors were assumed to follow a Gaussian distribution.

---

[16] Second-generation is used here to refer to stars in VVV CL001 that display altered light-element abundances (e.g., He, C, N, O, Na, Al, and Mg), which are different from those of typical MW field stars.
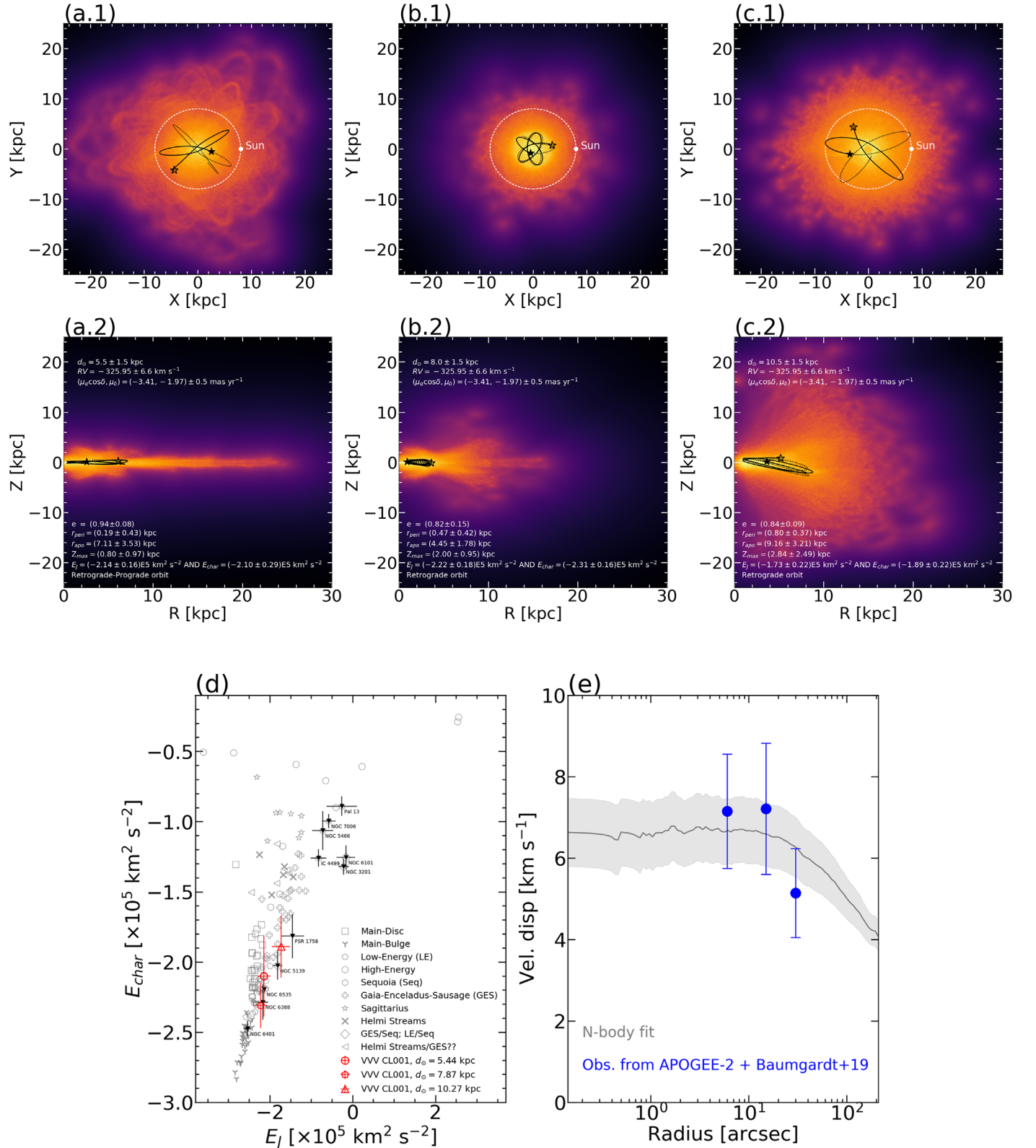
Figure 4. Ensemble of 10,000 orbits of VVV CL001, projected on the equatorial ((a.1), (b.1), and (c.1)) and meridional ((a.2), (b.2), and (c.2)) Galactic planes, in the inertial reference frame with a bar pattern speed of 41 km s⁻¹ kpc⁻¹, integrated over the past 2 Gyr. The red and orange colors correspond to more probable regions of the space, which are crossed most frequently by the simulated orbits. The black solid and dashed lines show the past and future orbits of VVV CL001, integrated over 200 Myr. The white dashed line indicates the Sun's radius. The filled and unfilled star symbols indicate the initial and final positions of the cluster, respectively. The main orbital elements are listed in panels ((a.2), (b.2), and (c.2)), with uncertainty ranges given by the 16th and 84th percentile values. Panel (d): the characteristic orbital energy ($E_{\rm char}$) vs. the orbital Jacobi constant (E_J) in the noninertial reference frame where the bar is at rest. The gray symbols refer to Galactic GCs associated with different progenitors, as suggested in Massari et al. ([2019](#)). VVV CL001 is shown with red open symbols, while other GCs (black triangles) associated to Seq and GES are highlighted for reference. Panel (e): line-of-sight velocity dispersion vs. radius for our target cluster stars from APOGEE-2 plus Baumgardt's data set (blue dots). The prediction of the best-fitting N-body model from Baumgardt & Hilker ([2018](#)) and Baumgardt et al. ([2019](#)) is shown as a solid gray line, and the light gray shaded region indicates the $1 - \sigma$ uncertainty from the fit.

To compute the orbits, we adopt a mean RV of -325.95 ± 6.6 km s^{-1} computed from the combined APOGEE-2 RVs of the two program stars and Holger Baumgardt's RV compilation[17] of 34 stars, which lie in the RV range between -341.13 and -310.22 km s^{-1}. From those stars, we select objects having a Renormalized Unit Weight Error below 1.4, as extracted from Gaia EDR3, which allows us to discard sources with problematic astrometric solutions (see, e.g., Lindegren et al. 2018). This reduces the 36 stars with RV information to 27 stars with both reliable proper motions and RV information, which were considered to compute the nominal proper motion of VVV CL001 after applying a $3 - \sigma$ clipping to the data, e.g., only 25 out of these 27 sources lie inside $3 - \sigma$ of the nominal proper motion of the cluster, as shown in panel (b) of Figure 1. From this procedure, the nominal proper motion of VVV CL001 is $(\mu_\alpha \cos(\delta), \mu_\delta) = (-3.41, -1.97)$ mas yr^{-1}, with an assumed uncertainty of 0.5 mas yr^{-1}. The heliocentric distance ($d_\odot$) of VVV CL001 remains uncertain; for this reason we assume three possible estimates (5.5, 8.0, and 10.5 kpc) close to the best isochrone fit, as shown in panel (f) of Figure 1.

The main orbital elements and the ensemble of orbits of VVV CL001 are displayed in panels (a) to (c) and (d) of Figure 4. The orbital parameters reveal that VVV CL001 lies on a radial and highly eccentric (>0.8) halo-like orbit with rather small excursions above the Galactic plane ($Z_{\max} < 3$ kpc), and pericentric (r_{peri}) distances below 1 kpc. We also find that VVV CL001 exhibits a retrograde and prograde sense at the same time when assuming a close heliocentric distance, while it is exclusively retrograde at and beyond the Bulge, similar to other GCs in the inner Galaxy (see Pérez-Villegas et al. 2020). Therefore, a more robust heliocentric distance estimation will better constrain these dynamics scenarios.

Panel (d) of Figure 4 shows that the orbital energy configuration of VVV CL001 is comparable to that of Galactic GCs associated with the major accretion events such as Sequoia (Seq.) and GES (see, e.g., Myeong et al. 2018; Massari et al. 2019), indicating that VVV CL001 could be the fossil relic of one of these accreted dwarf galaxies.

5. Mass

Baumgardt & Hilker (2018) performed N-body simulations of star clusters, and found that they could reproduce the surface-density profile of VVV CL001, finding a present-day mass of $9 \times 10^4 \, M_\odot$.

With the available RV data, we match the line-of-sight dispersion profiles to the N-body simulations of VVV CL001, as shown in panel (e) of Figure 4, and thus determine the most likely mass of the cluster from kinematics constraint. We adopted three radial bins (with bin centers of $6'$, $15'$, and $30'$), chosen to ensure that at least 10 stars were in each bin; resulting in the three blue dots shown in panel (e) of Figure 4. With the new data in panel (e) of Figure 4, we find $\sigma_0 \sim 6.6$ km s^{-1}. This yields a present-day estimated mass of $\sim 2.1 \times 10^5 \, M_\odot$, which suggests that VVV CL001 is two times more massive than previously thought, and approximately four times more massive than ESO280-SC06 (the most metal-poor GC known in the MW).

6. Concluding Remarks

We have performed the first near-IR high-resolution spectral analysis of two likely members of the GC VVV CL001, a cluster obscured by the heavy extinction and high field-star density in the direction of the Galactic Bulge. Based on high S/N APOGEE spectra, we measure a mean [Fe/H] metallicity of -2.45 ± 0.1, which makes VVV CL001 possibly the most metal-poor GC known, only slightly higher than ESO280-SC06 at -2.48.

VVV CL001 is very close in projection to UKS 1, which motivated Minniti et al. (2011) to suggest the possibility that they could be gravitationally bound. However, the RV of VVV CL001 is too large, and the orbits are very different, which allows us to rule out the binary-cluster scenario.

We find that the α-element abundances of VVV CL001 are typical of the lowest metallicity GCs known. Spectra for more members are required in order to confirm the presence of MPs in this cluster.

For the derivation of the age and reddening, we employed the new code SIRIUS (Souza et al. 2020). As shown in panel (e) of Figure 1, we derived a median age of $\sim 11.9^{+3.12}_{-4.05}$ Gyr, indicating that the very metal-poor GC VVV CL001 is among the oldest and most massive ($\sim 2.1 \times 10^5 \, M_\odot$) MW clusters.

A dynamical analysis of VVV CL001 reveals that this object has a radial and highly eccentric halo-like orbit confined inside the Sun's galactocentric distance. Both its metallicity and orbit favor the interpretation of VVV CL001 being a GC that belongs to an early accretion event in the MW corresponding to the either the Seq or GES dwarf galaxies. Finally, multiband photometry in the near-IR will be useful to identify other stellar tracers, such as RR Lyrae stars (if any) toward VVV CL001, which will significantly help to constrain the distance, age, and origin of the cluster.

ORCID iDs

José G. Fernández-Trincado ⓘ https://orcid.org/0000-0003-3526-5052
Dante Minniti ⓘ https://orcid.org/0000-0002-7064-099X
Stefano O. Souza ⓘ https://orcid.org/0000-0001-8052-969X
Timothy C. Beers ⓘ https://orcid.org/0000-0003-4573-6233
Doug Geisler ⓘ https://orcid.org/0000-0002-3900-8208
Sandro Villanova ⓘ https://orcid.org/0000-0001-6205-1493
Steven R. Majewski ⓘ https://orcid.org/0000-0003-2025-3147
Beatriz Barbuy ⓘ https://orcid.org/0000-0001-9264-4417
Angeles Pérez-Villegas ⓘ https://orcid.org/0000-0002-5974-3998
Lady Henao ⓘ https://orcid.org/0000-0002-2036-2944
María Romero-Colmenares ⓘ https://orcid.org/0000-0001-6515-5036
Alexandre Roman-Lopes ⓘ https://orcid.org/0000-0002-1379-4204

References

Ahumada, R., Allende Prieto, C., Almeida, A., et al. 2020, ApJS, 249, 3
Baumgardt, H., & Hilker, M. 2018, MNRAS, 478, 1520
Baumgardt, H., Hilker, M., Sollima, A., & Bellini, A. 2019, MNRAS, 482, 5138
Blanton, M. R., Bershady, M. A., Abolfathi, B., et al. 2017, AJ, 154, 28
Bowen, I. S., & Vaughan, A. H., Jr. 1973, ApOpt, 12, 1430
Cardelli, J. A., Clayton, G. C., & Mathis, J. S. 1989, ApJ, 345, 245
Dotter, A., Chaboyer, B., Jevremović, D., et al. 2008, ApJS, 178, 89
Fernández-Trincado, J. G., Beers, T. C., & Minniti, D. 2020a, A&A, 644, A83
Fernández-Trincado, J. G., Beers, T. C., Minniti, D., et al. 2020b, A&A, 643, L4
Fernández-Trincado, J. G., Beers, T. C., Minniti, D., et al. 2020c, ApJL, 903, L17
Fernández-Trincado, J. G., Beers, T. C., Placco, V. M., et al. 2019a, ApJL, 886, L8
Fernández-Trincado, J. G., Beers, T. C., Tang, B., et al. 2019b, MNRAS, 488, 2864
Fernández-Trincado, J. G., Chaves-Velasquez, L., Pérez-Villegas, A., et al. 2020d, MNRAS, 495, 4113
Fernández-Trincado, J. G., Mennickent, R., Cabezas, M., et al. 2019c, A&A, 631, A97
Fernández-Trincado, J. G., Minniti, D., Beers, T. C., et al. 2020e, A&A, 643, A145
Fernández-Trincado, J. G., Zamora, O., Souto, D., et al. 2019d, A&A, 627, A178
Gaia Collaboration, Brown, A. G. A., Vallenari, A., et al. 2020, A&A, in press
García Pérez, A. E., Allende Prieto, C., Holtzman, J. A., et al. 2016, AJ, 151, 144
Garro, E. R., Minniti, D., Gómez, M., et al. 2020, A&A, 642, L19
Geisler, D., Piatti, A. E., Claria, J. J., & Minniti, D. 1995, AJ, 109, 605
Gonzalez, O. A., Rejkuba, M., Zoccali, M., et al. 2012, A&A, 543, A13
Gonzalez, O. A., Rejkuba, M., Zoccali, M., Valenti, E., & Minniti, D. 2011, A&A, 534, A3
Gunn, J. E., Siegmund, W. A., Mannery, E. J., et al. 2006, AJ, 131, 2332
Harris, W. E. 1996, AJ, 112, 1487
Holtzman, J. A., Hasselquist, S., Shetrone, M., et al. 2018, AJ, 156, 125
Kruijssen, J. M. D. 2019, MNRAS, 486, L20
Larsen, S. S., Romanowsky, A. J., Brodie, J. P., & Wasserman, A. 2020, arXiv:2010.07395
Lindegren, L., Hernández, J., Bombrun, A., et al. 2018, A&A, 616, A2
Majewski, S. R., Schiavon, R. P., Frinchaboy, P. M., et al. 2017, AJ, 154, 94
Massari, D., Koppelman, H. H., & Helmi, A. 2019, A&A, 630, L4
Masseron, T., García-Hernández, D. A., Mészáros, S., et al. 2019, A&A, 622, A191
Masseron, T., Merle, T., & Hawkins, K. 2016, BACCHUS: Brussels Automatic Code for Characterizing High accUracy Spectra, Astrophysics Source Code Library, ascl:1605.004
Mészáros, S., Martell, S. L., Shetrone, M., et al. 2015, AJ, 149, 153
Mészáros, S., Masseron, T., García-Hernández, D. A., et al. 2020, MNRAS, 492, 1641
Minniti, D., Alonso-García, J., Braga, V., et al. 2017a, RNAAS, 1, 16
Minniti, D., Geisler, D., Alonso-García, J., et al. 2017b, ApJL, 849, L24
Minniti, D., Hempel, M., Toledo, I., et al. 2011, A&A, 527, A81
Minniti, D., Lucas, P. W., Emerson, J. P., et al. 2010, NewA, 15, 433
Myeong, G. C., Evans, N. W., Belokurov, V., Sanders, J. L., & Koposov, S. E. 2018, ApJL, 863, L28
Nidever, D. L., Holtzman, J. A., Allende Prieto, C., et al. 2015, AJ, 150, 173
Palma, T., Minniti, D., Alonso-García, J., et al. 2019, MNRAS, 487, 3140
Pérez-Villegas, A., Barbuy, B., Kerber, L. O., et al. 2020, MNRAS, 491, 3251
Planck Collaboration, Ade, P. A. R., Aghanim, N., et al. 2016, A&A, 594, A13
Sanders, J. L., Smith, L., & Evans, N. W. 2019, MNRAS, 488, 4552
Schiavon, R. P., Johnson, J. A., Frinchaboy, P. M., et al. 2017, MNRAS, 466, 1010
Simpson, J. D. 2018, MNRAS, 477, 4565
Smith, L. C., Lucas, P. W., Kurtev, R., et al. 2018, MNRAS, 474, 1826
Souza, S. O., Kerber, L. O., Barbuy, B., et al. 2020, ApJ, 890, 38
Wan, Z., Lewis, G. F., Li, T. S., et al. 2020, Natur, 583, 768
Wilson, J. C., Hearty, F. R., Skrutskie, M. F., et al. 2019, PASP, 131, 055001
Zasowski, G., Cohen, R. E., Chojnowski, S. D., et al. 2017, AJ, 154, 198
Zasowski, G., Johnson, J. A., Frinchaboy, P. M., et al. 2013, AJ, 146, 81